Journal of Physics B: Atomic, Molecular and Optical Physics

PAPER

Probing strong-field two-photon transitions through dynamic interference

To cite this article: Attila Tóth and András Csehi 2021 *J. Phys. B: At. Mol. Opt. Phys.* **54** 035005

IOP Publishing Journal of Physics B: Atomic, Molecular and Optical Physics
J. Phys. B: At. Mol. Opt. Phys. **54** (2021) 035005 (8pp) https://doi.org/10.1088/1361-6455/abdb8e

Probing strong-field two-photon transitions through dynamic interference

Attila Tóth[1] **and András Csehi**[2,*]

[1] ELI-ALPS, ELI-HU Non-Profit Ltd., H-6720 Szeged, Dugonics tér 13, Hungary
[2] Department of Theoretical Physics, University of Debrecen, H-4002 Debrecen, PO Box 400, Hungary

E-mail: csehi.andras@science.unideb.hu

Received 1 December 2020, revised 6 January 2021
Accepted for publication 13 January 2021
Published 15 February 2021

Abstract

We demonstrate how strong-field multiphoton transitions between dynamically shifted atomic levels can be traced in the energy spectra of emitted photoelectrons. Applying an ultrafast and intense laser pulse, two-photon Rabi oscillations are induced between two bound states of an atom. A third photon from the same pulse directly ionizes the atom, thus the emitted photoelectrons coherently probe the underlying dynamics. As the instantaneous energy of photoelectrons follows the pulse intensity envelope, modulated by the ac Stark shifts, electrons emitted with the same energy but at different times—at the rising and falling edge of the pulse—will interfere leading to pronounced dynamic interference pattern in the spectra. We investigate this phenomenon both numerically and analytically by developing a minimal three-state model that incorporates two-photon coupling and dynamically shifted atomic levels. On the example of atomic lithium ($2s \rightarrow\rightarrow 4s \rightarrow$ continuum) we show how the individual ac Stark shifts and the two-photon Rabi frequency are reflected through the asymmetry, shifting and splitting of the interference structure of the computed photopeaks.

Keywords: two-photon transition, strong-field ionization, dynamic interference, Stark shift

(Some figures may appear in colour only in the online journal)

1. Introduction

Coherent control of light–matter interactions induced by ultrafast and intense laser pulses has attracted much interest over the past decades. Several quantum control strategies have been proposed to steer the evolution of atomic and molecular processes along desired pathways including selective population transfer, ionization or photodissociation [1–5]. The stimulated Raman adiabatic passage (STIRAP) and related techniques were found very robust for efficient population transfer when the transitions are induced by a single photon.

It is well known, however, that in the strong-field regime where multiphoton transitions occur, the atomic and molecular levels are subject to ac Stark shifts which significantly modify the underlying physics [6, 7]. Numerous experimental and theoretical works have shown that despite the movement of the atomic levels, efficient population transfer is possible between two electronic states upon absorption of multiple photons from the same pulse [8–21]. In the majority of these works, two-photon transitions are considered in alkali metals and a proper modulation of the phase or shape of the laser pulse is applied to compensate the relative dynamic Stark shift (DSS) of interest. Although, transform limited (TL) pulses set to exact two-photon resonance are not optimal for efficient population transfer [8], by a proper blue or red detuning (depending on the sign of the relative DSS) one can achieve notable excitation even with TL pulses [11, 20].

Multiphoton excitation and subsequent ionization of atomic systems in the optical regime have been widely studied already from the eighty's [22–29]. The oscillatory patterns observed in the photoelectron spectra were attributed to Stark shifted bound state multiphoton transient resonances that give rise to interference of electron amplitudes generated on the rising and falling edge of the pulse. The first unambiguous observation of the interference of photoelectrons emitted at different times within the same pulse was made by Jones [28] who

* Author to whom any correspondence should be addressed.

used unfocused beams to avoid the spatial intensity variation effects of the laser which would otherwise make the process unobservable.

A very transparent illustration of the emergence of interference patterns found in sequential two-photon ionization spectra was given in reference [30] and later confirmed by direct wave packet propagations [31]. The resonantly coupled bound states subjected to a time-dependent coupling by the laser repel each other, and their time-dependent energies follow the pulse envelope. During the interaction with the laser, electrons emitted at the rising edge of the pulse have the same energy as those emitted at the falling edge. As a consequence, photoelectrons ejected with the same energy but with a time delay give rise to pronounced interference pattern in the spectrum. This dynamic interference of photoelectrons is a general phenomenon in strong-field processes as long as short laser pulses of high carrier frequency are considered and particles are emitted during the action of the pulse [30].

Originally, dynamic interference was demonstrated in the direct ionization of atomic systems exposed to high-intensity lasers in the XUV regime [32–40]. Especially, atomic hydrogen and helium were investigated in detail and it was shown that due to the strong ac Stark effect in the continuum, single peaks are replaced by multi-peak pattern in the spectrum [34]. Later, the ionization of hydrogen was revisited more accurately, and the essential conditions for dynamic interference have been specified [38]. After all, it became clear that ground state atoms exhibit dynamic interference, the onset of which can be considered as a signature of atomic stabilization [39]. Over the past years, further theoretical works have demonstrated the importance of dynamic interference from different perspectives [41–47], though an experimental realization is yet to be presented.

Dynamic interference in the multiphoton optical regime ($\omega < I_p$) is different from that found in direct ionization by intense high frequency lasers ($\omega > I_p$). In the former case, several high-lying excited states may be populated during the ionization process, furthermore these states might induce notable ac Stark shifts. As the ionization is rather efficient in that region [48], Rabi oscillations between bound states can be depleted and the interference pattern might wash out [38]. The application of longer pulses can help overcome these difficulties. Owing to the narrow bandwidth of such pulses, ionization is possible through selectively populated intermediate resonant states. Furthermore, the larger pulse duration allows one to use lower intensities, with which the peak values of the ac Stark shifts can be limited such that the interference pattern remain observable in the spectrum.

In the present work, we investigate such phenomena by considering the 2 + 1 photon resonance-enhanced multiphoton ionization of an atom in the strong-field regime, where DSSs start to play a role. Two-photon Rabi oscillations induced between two bound states of the atom are probed by a third photon leading to the emission of an electron. By developing a minimal three-state model that includes ac Stark shifts and multiphoton coupling, we numerically calculate the spectrum which exhibits multi-peak dynamic interference pattern. After deriving an analytical expression for the spectrum which nicely reproduces the numerical results, we reveal the impact of the individual Stark shifts, the two-photon Rabi frequency and the laser detuning on the asymmetry, splitting and shifting of the obtained spectra. For our analysis, we consider atomic lithium which has been intensively studied recently [49–57]. Our scheme in this work involves the $2s \rightarrow\rightarrow 4s \rightarrow$ continuum pathway for Li, but similar situations occur e.g. in other alkali metals.

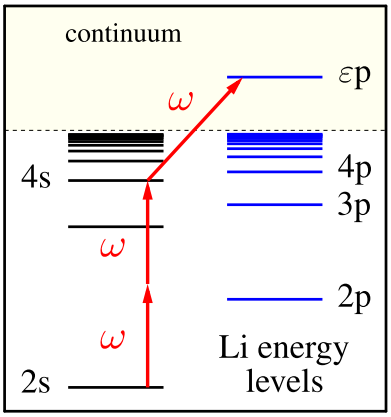

Figure 1. Energy level scheme of atomic lithium. Shown is the 2 + 1 photon resonance-enhanced ionization of Li from the 2s initial state ($|I\rangle$) to the εp final continuum state ($|\varepsilon\rangle$) mediated by the 4s resonant state ($|R\rangle$).

2. Theory

We start by introducing the theoretical framework for the strong-field 2 + 1 photon resonance-enhanced ionization process studied in this work. We consider atomic lithium as a concrete example initially in the 2s ground state ($|I\rangle$). Applying a coherent intense laser pulse, the system is excited by two photons to the 4s resonant state ($|R\rangle$) and then ionized by a single photon (see figure 1). The field-free atom is represented by the $\hat{H}_0$ Hamiltonian and its corresponding $|j\rangle$ eigenstates and ω_j eigenenergies ($\hbar = 1$), where the j index runs over the bound and continuum states. The interaction of the atom with the laser pulse is treated in the dipole approximation, that is $\hat{V}(t) = -\vec{\mu}\vec{\mathcal{E}}(t)$ where $\vec{\mu}$ is the transition dipole vector and $\vec{\mathcal{E}}(t)$ is the linearly polarized electric field. Throughout this work, Gaussian laser pulses of the form $\mathcal{E}(t) = \mathcal{E}_0 g(t)\cos(\omega t + \gamma(t))$ are applied, where $\mathcal{E}_0$ is the electric field amplitude, ω is the central angular frequency, and $g(t) = e^{-t^2/2\tau^2}$ is the envelope function with τ being the pulse duration that is closely related to the full width at half maximum (FWHM) FWHM $= 2\tau\sqrt{\ln 2}$. For simplicity, the $\gamma(t)$ phase of the field is kept constant ($\gamma = 0$) unless otherwise stated.

In the total time-dependent wave function of the system both the essential and nonessential states are explicitly included, and it reads [58]

$$\Psi(t) = c_I(t)|I\rangle e^{-i\omega_I t} + c_R(t)|R\rangle e^{-i\omega_R t} + \sum_m c_m(t)|m\rangle e^{-i\omega_m t} + \int c_\varepsilon(t)|\varepsilon\rangle e^{-i\omega_\varepsilon t} d\omega_\varepsilon. \quad (1)$$

In equation (1), the initial and resonant states (2s and 4s in case of Li) are denoted as $|I\rangle$ and $|R\rangle$, respectively, while the final continuum states which are populated after the ionization process, are labeled by $|\varepsilon\rangle$. The nonessential $|m\rangle$ states are dipole coupled to $|I\rangle$ and $|R\rangle$ but as they are far from resonance, their population is negligible during the atom–field interaction. The impact of these states on the studied two-photon transition is crucial as they give rise to the DSSs of the 2s and 4s levels to be discussed below. We note here that both the m- and ε-state manifold consists of p states ($l = 1$) in the present case due to the selection rules for the angular momentum.

After inserting equation (1) into the time-dependent Schrödinger-equation $i\dot{\Psi} = [\hat{H}_0 + \hat{V}(t)]\Psi$ we arrive at the full set of coupled differential equations for the $c_j(t)$ complex amplitudes

$$i\dot{c}_j(t) = \sum_k c_k(t)\, e^{-i\omega_{kj}t} V_{jk}(t), \tag{2}$$

where $\omega_{kj} = \omega_k - \omega_j$ $(j,k = I,R,m,\varepsilon)$ and the light–matter interaction term is written as $V_{jk}(t) = -\mathcal{E}(t)\mu_{jk}$ with $\mu_{jk} = \langle j|\hat{z}|k\rangle$ being the transition dipole moment (TDM) matrix element between the corresponding eigenstates of the atom. Equation (2) can be substantially simplified by invoking that the μ_{IR}, $\mu_{mm'}$ and $\mu_{m\varepsilon}$ TDMs are inherently zero, furthermore continuum–continuum transitions are ignored as we focus on the first photopeak in this study. After applying these considerations and also exploiting that direct ionization of the ground state is negligible for the considered photon energies, equation (2) is written as

$$i\dot{c}_I(t) = \sum_m c_m(t)\, e^{i\omega_{Im}t} V_{Im}(t) \tag{3a}$$

$$i\dot{c}_R(t) = \sum_m c_m(t)\, e^{i\omega_{Rm}t} V_{Rm}(t) + \int c_\varepsilon(t)\, e^{i\omega_{R\varepsilon}t} V_{R\varepsilon}(t) d\omega_\varepsilon \tag{3b}$$

$$i\dot{c}_m(t) = c_I(t)\, e^{-i\omega_{Im}t} V_{mI}(t) + c_R(t)\, e^{-i\omega_{Rm}t} V_{mR}(t) \tag{3c}$$

$$i\dot{c}_\varepsilon(t) = c_R(t)\, e^{-i\omega_{R\varepsilon}t} V_{\varepsilon R}(t). \tag{3d}$$

The last term in equation (3b) can be calculated explicitly by invoking the rotating wave approximation (RWA) and the local approximation [59]

$$\int c_\varepsilon(t)\, e^{i\omega_{R\varepsilon}t} V_{R\varepsilon}(t) d\omega_\varepsilon = -\frac{i}{2}\Gamma(t) c_R(t) \tag{4}$$

where $\Gamma(t) = \Gamma_0 g^2(t)$ with $\Gamma_0 = 2\pi|\mu_{R\varepsilon}\mathcal{E}_0/2|^2$ being the total rate for the ionization of the $|R\rangle$ resonant state. The right-hand side of equation (3d) can be also simplified using the RWA,

$$c_R(t)\, e^{-i\omega_{R\varepsilon}t} V_{\varepsilon R}(t) = c_R(t)\Omega_1(t)\, e^{i\delta t}, \tag{5}$$

where $\Omega_1(t) = -\frac{1}{2}\mu_{\varepsilon R}\mathcal{E}_0 g(t) = \Omega_1^0 \cdot g(t)$ and $\delta = \omega_{\varepsilon R} - \omega$ are the one-photon Rabi frequency and detuning, respectively.

To uncover the overall impact of the nonessential m-state manifold, we turn to equation (3c). As the offresonant intermediate states rapidly oscillate, the time evolution of the $c_m(t)$ amplitudes can be obtained by adiabatic elimination [11]. After integrating equation (3c) by parts and omitting small terms, we arrive at an explicit expression for the $c_m(t)$ amplitudes

$$\begin{aligned} c_m(t) = {} & \frac{\mu_{mI}}{2} c_I(t)\mathcal{E}_0 g(t) \left[\frac{e^{-i(\omega_{Im}+\omega)t}}{\omega_{mI}-\omega} + \frac{e^{-i(\omega_{Im}-\omega)t}}{\omega_{mI}+\omega}\right] \\ & + \frac{\mu_{mR}}{2} c_R(t)\mathcal{E}_0 g(t) \left[\frac{e^{-i(\omega_{Rm}+\omega)t}}{\omega_{mR}-\omega} + \frac{e^{-i(\omega_{Rm}-\omega)t}}{\omega_{mR}+\omega}\right] \end{aligned} \tag{6}$$

which is valid as long as the detuning of the $|m\rangle$ states is large compared to the pulse bandwidth, the two-photon detuning and the Stark shifts of interest. Inserting equation (6) into equations (3a) and (3b), and applying the two-photon RWA, that is dropping rapidly oscillating terms again, the following three-state equation is obtained

$$i\dot{c}_I(t) = S_I(t)c_I(t) + \Omega_2^\dagger(t)\, e^{-i\Delta t} c_R(t), \tag{7a}$$

$$i\dot{c}_R(t) = \Omega_2(t)\, e^{i\Delta t} c_I(t) + \left[S_R(t) - \frac{i}{2}\Gamma(t)\right] c_R(t), \tag{7b}$$

$$i\dot{c}_\varepsilon(t) = c_R(t)\Omega_1(t)\, e^{i\delta t}, \tag{7c}$$

where $\Delta = \omega_R - \omega_I - 2\omega$ is the two-photon detuning, $\Omega_2(t)$ is the two-photon Rabi frequency (assumed real)

$$\Omega_2(t) = -\sum_m \frac{\mu_{Rm}\cdot\mu_{mI}}{4} \frac{\mathcal{E}_0^2 g^2(t)}{\omega_{mI}-\omega} = \Omega_2^0 \cdot g^2(t) \tag{8}$$

and $S_k(t)$ is the DSS of the kth level ($k = I, R$) originating from the nonessential m-state manifold

$$S_k(t) = -\sum_m \frac{|\mu_{km}|^2 \cdot \mathcal{E}_0^2 g^2(t)}{2} \frac{\omega_{mk}}{\omega_{mk}^2 - \omega^2} = S_k^0 \cdot g^2(t). \tag{9}$$

We note here that both $\Omega_2(t)$ and $S_k(t)$ follow the $g^2(t)$ intensity profile of the pulse in accordance with previous studies [11, 15]. In equations (7a)–(7c), it is possible to eliminate the oscillating factors $e^{\pm i\Delta t}$ and $e^{i\delta t}$ by redefining the amplitudes as $c_R(t) \to c_R(t)e^{i\Delta t}$ and $c_\varepsilon(t) \to c_\varepsilon(t)e^{i(\Delta+\delta)t}$. After applying these changes and incorporating the $U_\mathrm{p}(t) = \mathcal{E}_0^2 \cdot g^2(t)/4\omega^2$ ponderomotive shift of the continuum, we arrive at our final equation

$$i\begin{pmatrix}\dot{c}_I(t)\\ \dot{c}_R(t)\\ \dot{c}_\varepsilon(t)\end{pmatrix} = \begin{pmatrix} S_I(t) & \Omega_2^\dagger(t) & 0 \\ \Omega_2(t) & \Delta + S_R(t) - \frac{i}{2}\Gamma(t) & 0 \\ 0 & \Omega_1(t) & \Delta + \delta + U_\mathrm{p}(t)\end{pmatrix} \times \begin{pmatrix} c_I(t)\\ c_R(t)\\ c_\varepsilon(t)\end{pmatrix} \tag{10}$$

Equation (10) describes the underlying physics investigated in this work. The strongly coupled $|I\rangle$ and $|R\rangle$ states undergo two-photon Rabi floppings governed by $\Omega_2(t)$, meanwhile the energy levels follow the intensity profile of the pulse through the $S_I(t)$ and $S_R(t)$ Stark shifts. This two-photon Rabi dynamics is probed by a third photon from the same pulse leading to the emission of an electron. The leakage of the population of the $|R\rangle$ resonant state is described by the $-\frac{i}{2}\Gamma(t)$ imaginary term, while the single-photon coupling to the continuum is dictated by $\Omega_1(t)$. Inclusion of the time-dependent $U_\mathrm{p}(t)$ ponderomotive

shift of the continuum levels is essential as it approximately gives rise to the Stark shifts in the continuum [38]. $U_p(t)$ is expected to cause additional shift of the spectral peaks by raising the I_p ionization potential [23, 60, 61], and also to affect the interference of electrons emitted at different times.

In the next section, equation (10) will be used for the numerical investigation of the (2 + 1) photon ionization of atomic lithium. After applying analytical considerations to equation (10) a direct link between the computed spectra and the $\Omega_2(t)$, $S_k(t)$, Δ and $U_p(t)$ quantities will be demonstrated.

3. Results

In what follows, we investigate the strong-field multiphoton ionization of ground state Li atoms induced by an intense short laser pulse in the optical regime. The time evolution of the laser-driven system is obtained by solving equation (10) which describes the 2 + 1 photon resonance-enhanced ionization process under consideration. To calculate the necessary frequency dependent quantities in equation (10), such as the $S_I(t)$ and $S_R(t)$ energy shifts, the $\Omega_1(t)$ and $\Omega_2(t)$ Rabi frequencies and the $\Gamma(t)$ total rate for the ionization, the energy levels and TDMs of Li have been evaluated. The bound state energies and wave functions have been obtained by the direct diagonalization of the single-active-electron Hamiltonian of Li [49] discretized on a finite-element discrete-variable representation grid [62] while those of the continuum states with the Numerov method, and an excellent agreement has been found with previous results in terms of energy levels and TDMs [63, 64]. The bare energy difference between the 2s and 4s states is found $\omega_{RI} = 0.15944$ a.u. ≈ 4.339 eV while the peak values for the dynamical quantities of interest are obtained as $S_I^0 = 0.0193$ eV, $S_R^0 = 0.0077$ eV, $U_p^0 = 0.0071$ eV, $\Omega_1^0 = -0.0151$ eV, $\Omega_2^0 = -0.0078$ eV and $\Gamma_0 = 0.0005$ eV for $\Delta = 0$ (i.e. $\omega = \omega_{RI}/2$) and a typical laser intensity of $I_0 = 2.331 \times 10^{11}$ W cm^{-2} ($\mathcal{E}_0 = 0.002\,577$ a.u.). We note that the above values of the Stark shifts are in line with highly accurate *ab initio* data both for the 2s [65] and 4s states [66].

The numerical results of the time propagations obtained via equation (10) are shown in figure 2. Here the applied Gaussian laser pulse (FWHM = 1000 fs) is set to bare two-photon resonance for the 2s–4s transition ($\Delta = 0 \rightarrow \omega = \omega_{RI}/2 =$ 2.169 eV) and the laser intensity is varied such that several Rabi oscillations are induced meanwhile the total ionization remains far from saturation. As seen in the final populations ($p_k = |c_k(t \rightarrow \infty)|^2$) in figure 2(a), the system undergoes damped Rabi oscillations and completes more and more Rabi cycles as the laser intensity is increased, furthermore the ionization probability does not exceed 25% for the highest considered intensity. The corresponding photoelectron spectra calculated as $\sigma(\omega_\varepsilon) = |c_\varepsilon(t \rightarrow \infty)|^2$ is presented in figure 2(b) by a color map. Several interesting observations can be made in the intensity dependence of the spectrum. Upon increasing laser intensity, the position of the photopeak is shifted to higher energies relative to its nominal position in the weak-field limit ($\omega_{\varepsilon_0} = \omega_I + 3\omega = 1.117$ eV—horizontal dashed line in figure 2(b)). Furthermore, the photopeak gets

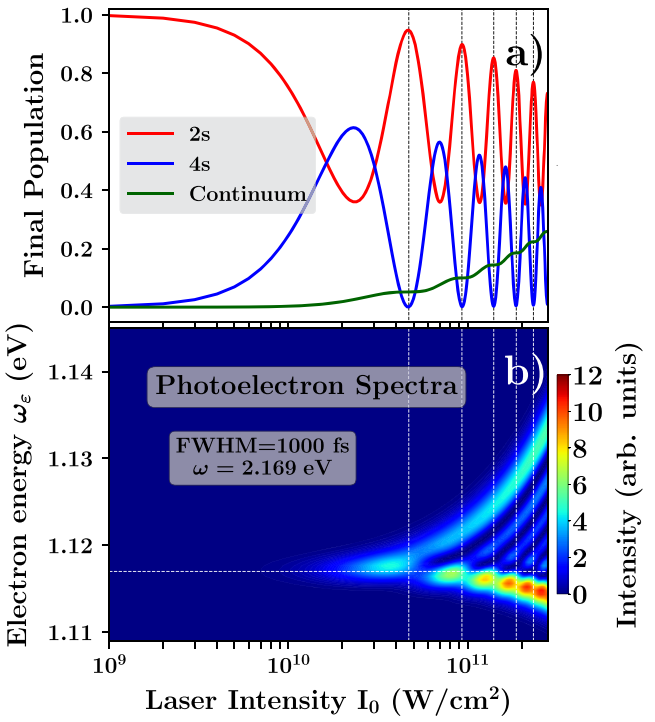

Figure 2. Resonance-enhanced 2 + 1 photon ionization of atomic Li induced by a Gaussian laser pulse (FWHM = 1000 fs) set to bare two-photon resonance for the 2s $\rightarrow\rightarrow$ 4s transition ($\Delta = 0$). (a) Final populations of the resonantly coupled 2s and 4s states as well as the total ionization probability are shown as a function of the laser intensity. Vertical dashed lines indicate the intensities at which the system completes integer number of Rabi cycles. (b) Photoelectron spectra computed for different laser intensities. Splitting of the main photopeak for increasing intensities is caused by the strong coupling with the laser, while the appearance of multi-peak structure is the result of dynamic interference. Owing to the atomic level Stark shifts, the spectrum is shifted from its nominal position in the weak-field limit (horizontal dashed line) and becomes asymmetric (see text for details). The presented results are obtained solving equation (10).

splitted and exhibits richer and richer multi-peak pattern as the laser-atom coupling is increased. Taking cuts at selected intensities in figure 2(b), it is seen that the main peaks are asymmetric with respect to their center and the number of subpeaks within each photopeak directly reflects the number of completed Rabi cycles. All these observations are attributed to dynamic interference of photoelectrons emitted with the same energy but at different times in the presence of dynamically shifted atomic levels.

In order to gain insight into the origin of the asymmetry, shifting and splitting of the interference pattern of the photopeaks, we would like to calculate analytically the time evolution of $c_\varepsilon(t)$ and then the spectrum as $\sigma(\omega_\varepsilon) = |c_\varepsilon(t \rightarrow \infty)|^2$. To do so, below we consider the picture of decoupled resonances which allows one to calculate the $c_\varepsilon(t)$ amplitudes [30]. We recall that the near-resonance transition between the $|I\rangle$ and $|R\rangle$ states in equation (10) is dictated by the 2×2 Hamiltonian

$$\hat{H}_{2ph}(t) = \begin{pmatrix} S_I(t) & \Omega_2^\dagger(t) \\ \Omega_2(t) & \Delta + S_R(t) - \dfrac{i}{2}\Gamma(t) \end{pmatrix}, \qquad (11)$$

where Δ can be tuned such that the $\delta S(t) = S_R(t) - S_I(t)$ relative DSS is roughly compensated during the action of the pulse (with chirped pulses $\delta S(t)$ can be compensated at each moment [12]).

Owing to the $-\frac{i}{2}\Gamma(t)$ lossy term, equation (11) gives rise to two decoupled resonances ($|+\rangle$ and $|-\rangle$), which are superpositions of the field-free atomic states ($|I\rangle$ and $|R\rangle$). Assuming that ionization is not dominant, i.e. $\Omega_2(t) \gg \frac{1}{2}\Gamma(t)$, and after introducing the sum of the individual Stark shifts, $\Sigma(t) = S_I(t) + S_R(t)$, the time-dependent energies and wave functions of the emerging resonances obtained by diagonalizing $\hat{H}_{2\mathrm{ph}}(t)$ are written as

$$E_\pm \simeq \frac{\Sigma(t)+\Delta}{2} \pm \sqrt{\Omega_2^2(t) + \left(\frac{\delta S(t)+\Delta}{2}\right)^2} - \frac{i}{4}\Gamma(t) \tag{12a}$$

$$|-\rangle \simeq \frac{1}{\sqrt{1+\left(\frac{\Lambda_-(t)}{\Omega_2(t)}\right)^2}}\left[|I\rangle + \left(\frac{\Lambda_-(t)}{\Omega_2(t)}\right)|R\rangle\right] \tag{12b}$$

$$|+\rangle \simeq \frac{1}{\sqrt{1+\left(\frac{\Lambda_+(t)}{\Omega_2(t)}\right)^2}}\left[|I\rangle + \left(\frac{\Lambda_+(t)}{\Omega_2(t)}\right)|R\rangle\right] \tag{12c}$$

$$\Lambda_\pm(t) = \frac{\delta S(t)+\Delta}{2} \pm \sqrt{\Omega_2^2(t) + \left(\frac{\delta S(t)+\Delta}{2}\right)^2}. \tag{12d}$$

We see that, because of the $(\Sigma(t)+\Delta)$ term in equation (12a) the energy splitting of the resonances is not symmetric with respect to zero, and because of $(\delta S(t)+\Delta)$ in equations (12b)–(12d) the resulting wave functions are not equally weighted superpositions of the bare atomic states. Clearly, when the Stark shifts are not relevant and the field is set to exact resonance ($\Delta = 0$), the arising resonance states are equally weighted superpositions of $|I\rangle$ and $|R\rangle$ with a symmetric energy splitting. Here, we focus on the more general case, when the dynamical shifts of atomic levels are relevant and non-zero detuning is applied to maintain resonance (or near-resonance) condition.

To proceed further, we first write the time-dependent amplitudes for the resonance states using the initial condition $c_\pm(t \to -\infty) = 1/\sqrt{2}$ and the expression for the energies (equation (12a))

$$c_\pm(t) = \frac{1}{\sqrt{2}} e^{-i\mathcal{R}_\pm(t)+\mathcal{I}(t)}, \tag{13}$$

where $\mathcal{R}_\pm(t) = \int_{-\infty}^{t} \mathrm{Re}\{E_\pm(t')\}dt'$ and $\mathcal{I}(t) = \int_{-\infty}^{t} \mathrm{Im}\{E_\pm(t')\}dt'$ are integrals of the real and imaginary parts of the energies, respectively. Next we express $|R\rangle$ from equations (12b) and (12c) and substitute equation (13) to arrive at the amplitude for the intermediate state

$$c_R(t) = \frac{1}{\sqrt{2}}\left(\frac{\Omega_2(t)}{\Lambda_+ - \Lambda_-}\right)\left\{\sqrt{1+\left(\frac{\Lambda_+(t)}{\Omega_2(t)}\right)^2}\, e^{-i\mathcal{R}_+(t)+\mathcal{I}(t)} - \sqrt{1+\left(\frac{\Lambda_-(t)}{\Omega_2(t)}\right)^2}\, e^{-i\mathcal{R}_-(t)+\mathcal{I}(t)}\right\}. \tag{14}$$

Using equation (14), it is possible to calculate $c_\varepsilon(t)$ (see e.g. reference [59]) and then the spectrum as $\sigma(\omega_\varepsilon) = |c_\varepsilon(t \to \infty)|^2$. By incorporating $U_\mathrm{p}(t)$ via its integral $u(t) = \int_{-\infty}^{t} U_\mathrm{p}(t')dt'$ we finally obtain for the spectrum

$$\sigma(\omega_\varepsilon) = \frac{1}{2}\left|\int_{-\infty}^{\infty}\left(\frac{\Omega_1(t)\Omega_2(t)}{\Lambda_+(t) - \Lambda_-(t)}\right) e^{\mathcal{I}(t)}\left\{\sqrt{1+\left(\frac{\Lambda_+(t)}{\Omega_2(t)}\right)^2} \times e^{i[(\Delta+\delta)t - \mathcal{R}_+(t)+u(t)]} - \sqrt{1+\left(\frac{\Lambda_-(t)}{\Omega_2(t)}\right)^2} \times e^{i[(\Delta+\delta)t - \mathcal{R}_-(t)+u(t)]}\right\} dt\right|^2 \tag{15}$$

where $\Delta + \delta = \omega_{\varepsilon I} - 3\omega$ is nothing but the total detuning relative to the $\omega_{\varepsilon_0} = \omega_I + 3\omega$ center of the spectrum.

$\sigma(\omega_\varepsilon)$ gives us the energy distribution of photoelectrons emitted after strong-field two-photon transition in the presence of dynamically shifted atomic levels. The formula is also valid when the field is not exactly in resonance. We note here that in case of vanishing Stark shifts and exact resonance ($\Delta = 0$), equation (15) is greatly simplified and the resulting spectrum is fully equivalent with that presented in reference [30] for resonant $1 + 1$ photon ionization processes. It is possible to further simplify equation (15) by invoking the stationary phase approximation [35] that is collecting terms that give the dominant contributions to $\sigma(\omega_\varepsilon)$. However, we would like to stop at this point and utilize equation (15) as it stands to find relation between the main features of the spectra and the most important quantities that characterize the underlying strong-field transition, namely the Stark shifts and the two-photon Rabi frequency.

To demonstrate the validity of $\sigma(\omega_\varepsilon)$, the photoelectron spectra calculated via equation (15) are presented in figure 3 by red lines. Here the same intensities are applied as shown by the vertical lines in figure 2 and for comparison the numerical results from equation (10) are also included either with $U_\mathrm{p}(t)$ or without $U_\mathrm{p}(t)$. Clearly, the most important properties of the spectra obtained with $U_\mathrm{p}(t)$—such as the asymmetry, shifting, splitting and the multi-peak pattern—are nicely reproduced by the formula computed in the picture of decoupled resonances. Importantly, the spectra computed with the $U_\mathrm{p}(t)$ ponderomotive shift of the continuum levels exhibit additional shifting and a modified interference pattern.

Let us further inspect the general formula in equation (15). As was shown above, $\sigma(\omega_\varepsilon)$ originates from the decoupled resonances $|+\rangle$ and $|-\rangle$, which are described by the first and second terms in the braces, respectively. The energies of these

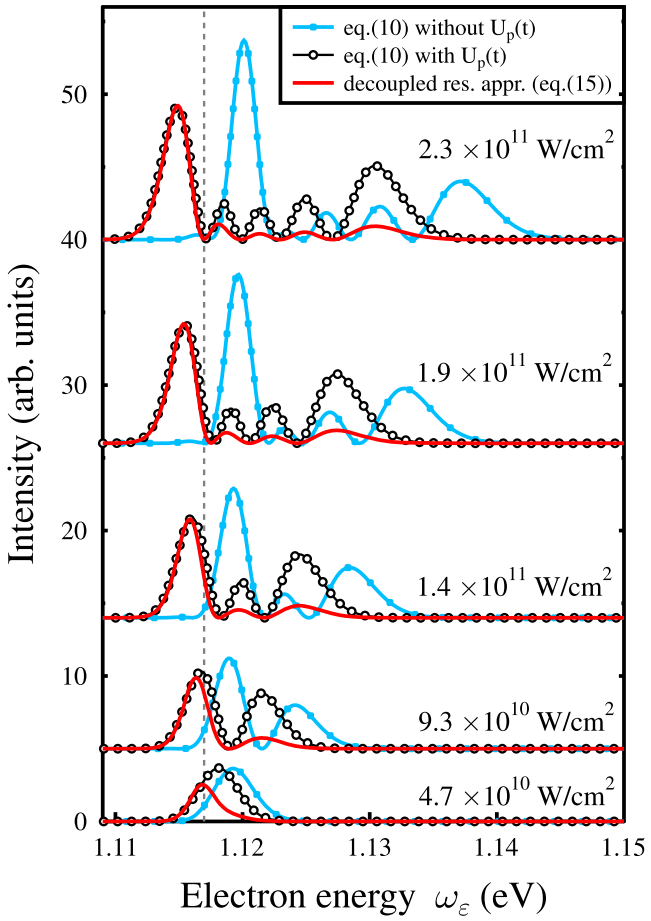

Figure 3. Photoelectron spectra of Li after the strong-field 2s–4s transition, computed numerically via equation (10) either with $U_p(t)$ (black lines with circles) or without $U_p(t)$ (blue lines) and given by the formula in equation (15) (red lines). The applied laser parameters are the same as in figure 2: FWHM = 1000 fs, $\omega = 2.169$ eV ($\Delta = 0$), and the intensities are chosen such that the system completes integer number of Rabi cycles (see also the vertical lines in figure 2). Note that the most important features of the spectra obtained with $U_p(t)$ -asymmetry, shifting, splitting and the multi-peak structure that is caused by dynamic interference—are nicely reproduced by the analytical results obtained in the picture of decoupled resonances. Importantly, the $U_p(t)$ ponderomotive shift of the continuum causes additional shift of the spectrum and modifies the interference pattern. For transparency, the individual spectra are vertically shifted apart from each other. The vertical dashed line indicates the nominal position of the spectrum.

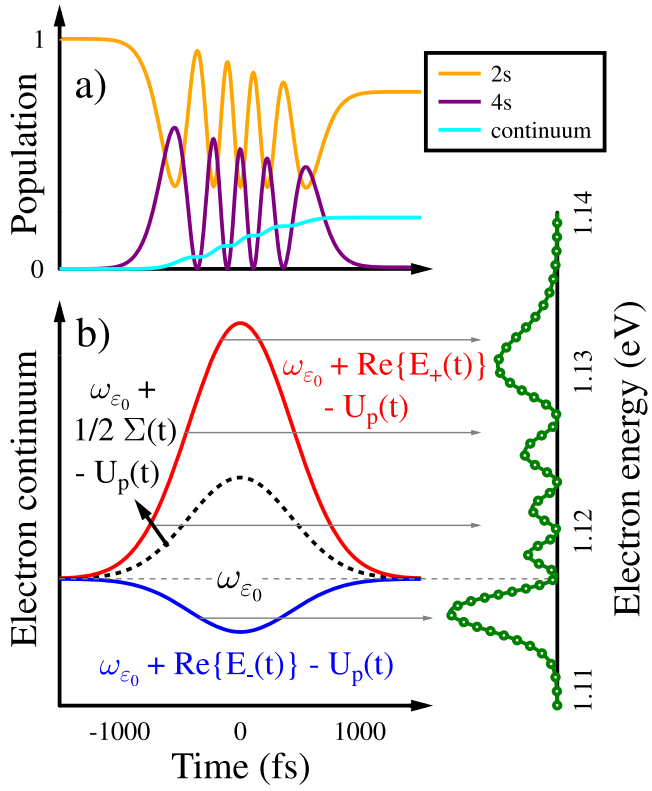

Figure 4. Strong-field ionization of Li induced by a two-photon resonant ($\Delta = 0$) laser pulse of $I_0 = 2.331 \times 10^{11}$ W cm^{-2} peak intensity and FWHM = 1000 fs duration. (a) The time-dependent populations of the 2s (orange line), 4s (purple line) and all the continuum states (cyan line) reveal that the system completes five Rabi cycles, meanwhile the total ionization caused by a third photon is below 25%. (b) The strong coupling of the 2s and 4s states caused by the laser gives rise to two decoupled resonances, the energies of which are given by equation (12a) and shown here by the red and blue lines relative to the nominal position of the photopeak $\omega_{\varepsilon_0} = \omega_I + 3\omega$ shifted by the $U_p(t)$ ponderomotive energy. The horizontal gray arrows symbolize electron amplitudes of particular energies that are emitted at the rising and falling edge of the pulse and cause the interference pattern in the spectrum shown on the right side by the green line.

resonances vary according to equation (12a) and are directly associated with the two sides of the spectrum ($E_-(t)$ with the lower-, and $E_+(t)$ with the higher energy side). Owing to the $(\delta S(t) + \Delta)$ dependence of $\Lambda_\pm(t)$, the exponentials have different prefactors. Consequently, the two sides of the photopeak are expected to differ in height leading to asymmetry in the spectrum. Furthermore, the total phases in the exponential factors, $\Phi_\pm(t) = (\Delta + \delta)t - \mathcal{R}_\pm(t) + u(t)$ are not symmetric due to the $(\Sigma(t) + \Delta)$ term in $\mathcal{R}_\pm(t)$, which suggests additional asymmetry and a shifting of the center of the spectrum. Looking at the time-dependent energy expressions of the resonances in equation (12a), we see that both $|-\rangle$ and $|+\rangle$ experience the same loss of $-\frac{i}{4}\Gamma(t)$, furthermore the real parts of $E_-(t)$ and $E_+(t)$ follow the $g^2(t)$ pulse intensity envelope below and above $\frac{1}{2}\Sigma(t)$ when $\Delta = 0$. This is illustrated in figure 4(b) for the $I_0 = 2.331 \times 10^{11}$ W cm^{-2} peak intensity case. Here, the time-dependent energies of the emerging resonances are shown by the blue and red lines relative to the $\omega_{\varepsilon_0} = \omega_I + 3\omega$ nominal center of the photopeak shifted by the $U_p(t)$ ponderomotive energy in the continuum. In this picture, the main features of the spectrum—shown by the green line in figure 4(b)—are easily understood. As the pulse arrives, the two resonances repel each other and the emitted electrons will gain energy in a wide interval giving rise to the splitting of the photopeak. After the pulse has reached its maximum and expires, the ejected electrons will have the same energies as those emitted at the rising edge of the pulse. Owing to the temporal difference of the electron amplitudes generated at the two sides of the pulse, pronounced interference pattern is observed in the spectrum. The number of sub-peaks within the main peak (in this case five) equals the number of Rabi cycles accomplished by the system (see figure 4(a)).

The degree of asymmetry, splitting and shifting of the center of the photopeaks are directly related to the peak values of the resonance energies, $E_-(t=0)$ and $E_+(t=0)$ and to $U_\mathrm{p}(t=0)$. As seen in figure 4(b), (i) the extent of splitting is linked to the difference of the peak resonance energies $\mathrm{Re}\{E_+(t=0)\} - \mathrm{Re}\{E_-(t=0)\}$; (ii) the shifting of the photopeak center relative to ω_{ε_0} is connected to the sum of the peak Stark shifts, $\frac{1}{2}\Sigma(t=0)$ minus the peak ponderomotive shift of the continuum levels, U_p^0; (iii) while the asymmetry is explained by the fact that the peak values of the resonance energies shifted by U_p^0 (and also the curvature of $\mathrm{Re}\{E_+(t)\} - U_\mathrm{p}(t)$ and $\mathrm{Re}\{E_-(t)\} - U_\mathrm{p}(t)$ at $t=0$) differ in magnitude, hence the energy distribution of emitted electrons on the two sides of the main photopeak differs in general.

In the concrete example of Li, the sum of the 2s and 4s Stark shifts is positive, thus the photopeak is shifted to larger energies relative to $\omega_{\varepsilon_0} - U_\mathrm{p}^0$. Furthermore, as the energy of $|-\rangle$ is lower in magnitude than that of $|+\rangle$, electrons ejected at the lower energy side of the photopeak are distributed in a narrow energy window in contrast to those emitted on the higher energy side. As a consequence, the lower energy side of the spectrum is higher than the higher energy side (see figure 4).

4. Conclusions

We have investigated the 2 + 1 photon resonance-enhanced strong-field ionization of an atom by developing a minimal three-state model that incorporates ac Stark shifts and multiphoton coupling. Based on the numerically obtained (equation (10)) photoelectron spectra that are qualitatively supported by the results of an analytical model presented here (equation (15)), we could show that dynamic interference of photoelectrons substantially modifies the spectrum when the resonantly coupled atomic levels are subject to dynamical shifts. On the example of Li, we have demonstrated that the strong resonant coupling of the 2s and 4s states induced by the laser gives rise to two decoupled resonances, the time-dependent energies of which repel each other and become responsible for the main features of the photopeaks (see figure 4). The asymmetry and shifting of the spectra are caused by the ac Stark shifts of the involved atomic levels, while the multi-peak structure results from dynamic interference of electron amplitudes generated at the rising and falling sides of the laser pulse.

To interpret the origin of the spectral characteristics, the picture of decoupled resonances was found very useful. The analytically obtained energies of the emerging resonances (equation (12a)) allows one to find relation between the main features of the spectra and the individual Stark shifts as well as the two-photon Rabi frequency. We have also shown that the time-dependent ponderomotive shift of the continuum levels not only shifts the position of the spectrum but modifies the dynamic interference pattern as the electrons entering the continuum at different times experience different energy shifts. The spectral characteristics discussed in this paper are general features in strong-field ionization processes where dynamical energy level shifts become prominent and should be observable in future experiments.

Data availability statement

The data that support the findings of this study are available upon reasonable request from the authors.

Acknowledgments

S Borbély is greatly acknowledged for valuable discussions. This research was supported by the EU-funded Hungarian Grant No. EFOP-3.6.2-16-2017-00005, and the ELI-ALPS Project GINOP 2.3.6-15-2015-00001.

ORCID iDs

Attila Tóth https://orcid.org/0000-0002-2161-316X
András Csehi https://orcid.org/0000-0002-8794-6610

References

[1] Tannor D J and Rice S A 1988 *Adv. Chem. Phys.* **70** 441
[2] Warren W S, Rabitz H and Dahleh M 1993 *Science* **259** 1581
[3] Bergmann K, Theuer H and Shore B W 1998 *Rev. Mod. Phys.* **70** 1003
[4] Shapiro M and Brumer P 2000 *Adv. At. Mol. Opt. Phys.* **42** 287
[5] Sussman B J, Townsend D, Ivanov M Y and Stolow A 2006 *Science* **314** 278
[6] Delone N B and Krainov V P 1999 *Phys.-Usp.* **42** 669
[7] Sussman B J 2011 *Am. J. Phys.* **79** 477
[8] Dudovich N, Dayan B, Gallagher Faeder S M and Silberberg Y 2001 *Phys. Rev. Lett.* **86** 47
[9] Rickes T, Yatsenko L P, Steuerwald S, Halfmann T, Shore B W, Vitanov N V and Bergmann K 2000 *J. Chem. Phys.* **113** 534
[10] Präkelt A, Wollenhaupt M, Sarpe-Tudoran C and Baumert T 2004 *Phys. Rev.* A **70** 063407
[11] Trallero-Herrero C, Cardoza D, Weinacht T C and Cohen J L 2005 *Phys. Rev.* A **71** 013423
[12] Trallero-Herrero C, Cohen J L and Weinacht T C 2006 *Phys. Rev. Lett.* **96** 063603
[13] Gandman A, Chuntonov L, Rybak L and Amitay Z 2007 *Phys. Rev.* A **75** 031401
[14] Haas M *et al* 2006 *Phys. Rev.* A **73** 052501
[15] Lee S, Lim J, Ahn J, Hakobyan V and Guérin S 2010 *Phys. Rev.* A **82** 023408
[16] Lee S, Lim J, Park C Y and Ahn J 2011 *Opt. Express* **19** 2266
[17] Astapenko V A and Sakhno S V 2016 *J. Mod. Opt.* **63** 2198
[18] Fushitani M *et al* 2016 *Nat. Photon.* **10** 102
[19] Bunjac A, Popović D B and Simonović N S 2017 *Phys. Chem. Chem. Phys.* **19** 19829
[20] Csehi A 2019 *J. Phys. B: At. Mol. Opt. Phys.* **52** 025002
[21] Nieddu T, Ray T, Rajasree K S, Roy R and Chormaic S N 2019 *Opt. Express* **27** 6528
[22] Rogus D and Lewenstein M 1986 *J. Phys. B: At. Mol. Phys.* **19** 3051
[23] Freeman R R, Bucksbaum P H, Milchberg H, Darack S, Schumacher D and Geusic M E 1987 *Phys. Rev. Lett.* **59** 1092
[24] Bardsley J N, Szöke A and Comella M J 1988 *J. Phys. B: At. Mol. Opt. Phys.* **21** 3899
[25] Reed V C and Burnett K 1991 *Phys. Rev.* A **43** 6217
[26] Story J G and Gallagher T F 1993 *Phys. Rev.* A **47** 5037
[27] Story J G, Duncan D I and Gallagher T F 1993 *Phys. Rev. Lett.* **70** 3012
[28] Jones R R 1995 *Phys. Rev. Lett.* **74** 1091
[29] Wickenhauser M, Tong X M and Lin C D 2006 *Phys. Rev.* A **73** 011401

[30] Demekhin P V and Cederbaum L S 2012 *Phys. Rev.* A **86** 063412
[31] Müller A D, Kutscher E, Artemyev A N, Cederbaum L S and Demekhin P V 2018 *Chem. Phys.* **509** 145
[32] Toyota K, Tolstikhin O I, Morishita T and Watanabe S 2007 *Phys. Rev.* A **76** 043418
Toyota K, Tolstikhin O I, Morishita T and Watanabe S 2008 *Phys. Rev.* A **78** 033432
[33] Tolstikhin O I 2008 *Phys. Rev.* A **77** 032712
[34] Demekhin P V and Cederbaum L S 2012 *Phys. Rev. Lett.* **108** 253001
[35] Demekhin P V and Cederbaum L S 2013 *Phys. Rev.* A **88** 043414
[36] Demekhin P V, Hochstuhl D and Cederbaum L S 2013 *Phys. Rev.* A **88** 023422
[37] Artemyev A N, Müller A D, Hochstuhl D, Cederbaum L S and Demekhin P V 2016 *Phys. Rev.* A **93** 043418
[38] Baghery M, Saalmann U and Rost J M 2017 *Phys. Rev. Lett.* **118** 143202
[39] Jiang W-C and Burgdörfer J 2018 *Opt. Express* **26** 19921
[40] Jiang W-C, Chen S-G, Peng L-Y and Burgdörfer J 2020 *Phys. Rev. Lett.* **124** 043203
[41] Wang M-X, Liang H, Xiao X-R, Chen S-G, Jiang W-C and Peng L-Y 2018 *Phys. Rev.* A **98** 023412
[42] Wang N and Liu A 2019 *Chin. Phys.* B **28** 083403
[43] Yu C, Fu N, Zhang G and Yao J 2013 *Phys. Rev.* A **87** 043405
[44] Yue L and Madsen L B 2014 *Phys. Rev.* A **90** 063408
[45] Yu C, Fu N, Hu T, Zhang G and Yao J 2013 *Phys. Rev.* A **88** 043408
[46] Zhang S B and Rohringer N 2014 *Phys. Rev.* A **89** 013407
[47] Marante C, Argenti L and Martín F 2014 *Phys. Rev.* A **90** 012506
[48] Kaiser B, Brand A, Glässl M, Vagov A, Axt V M and Pietsch U 2013 *New J. Phys.* **15** 093016
[49] Tumakov D A, Telnov D A, Plunien G and Shabaev V M 2019 *Phys. Rev.* A **100** 023407
[50] Murakami M, Zhang G P, Telnov D A and Chu S-I 2018 *J. Phys. B: At. Mol. Opt. Phys.* **51** 175002
[51] Liu F L and Zhao L B 2017 *Phys. Rev.* A **95** 043428
[52] Cohen S, Harb M M, Ollagnier A, Robicheaux F, Vrakking M J J, Barillot T, Lépine F and Bordas C 2016 *Phys. Rev.* A **94** 013414
[53] Schuricke M, Bartschat K, Grum-Grzhimailo A N, Zhu G, Steinmann J, Moshammer R, Ullrich J and Dorn A 2013 *Phys. Rev.* A **88** 023427
[54] Jheng S-D and Jiang T F 2013 *J. Phys. B: At. Mol. Opt. Phys.* **46** 115601
Jheng S-D and Jiang T F 2017 *J. Phys. B: At. Mol. Opt. Phys.* **50** 195001
[55] Morishita T and Lin C D 2013 *Phys. Rev.* A **87** 063405
[56] Schuricke M *et al* 2011 *Phys. Rev.* A **83** 023413
[57] Thini F *et al* 2020 *J. Phys. B: At. Mol. Opt. Phys.* **53** 095201
[58] Tannor D 2005 *Introduction to Quantum Mechanics: A Time-Dependent Perspective* (Mill Valley, CA: University Science Books)
[59] Demekhin P V and Cederbaum L S 2011 *Phys. Rev.* A **83** 023422
[60] Kopold R, Becker W, Kleber M and Paulus G G 2002 *J. Phys. B: At. Mol. Opt. Phys.* **35** 217
[61] Sándor P, Zhao A, Rozgonyi T and Weinacht T 2014 *J. Phys. B: At. Mol. Opt. Phys.* **47** 124021
[62] Borbély S, Tóth A, Arbó D G, Tökési K and Nagy L 2019 *Phys. Rev.* A **99** 013413
[63] Safronova M S, Safronova U I and Clark C W 2012 *Phys. Rev.* A **86** 042505
[64] Qi Y-Y, Wu Y, Wang J-G and Ding P-Z 2008 *Chin. Phys. Lett.* **25** 3620
[65] Tang L-Y, Bromley M W J, Yan Z-C and Mitroy J 2013 *Phys. Rev.* A **87** 032507
[66] Tang L-Y 2020 (unpublished)